



HAL
open science

Evaluation of LIF thermometry technique using Krypton as a tracer: Impact of laser lineshape and collisional bandwidth

Nathalie Lamoureux, Pradeep Parajuli, Waruna Kulatilaka, Pascale Desgroux

► **To cite this version:**

Nathalie Lamoureux, Pradeep Parajuli, Waruna Kulatilaka, Pascale Desgroux. Evaluation of LIF thermometry technique using Krypton as a tracer: Impact of laser lineshape and collisional bandwidth. Proceedings of the Combustion Institute, 2023, 39 (1), pp.1239-1248. 10.1016/j.proci.2022.07.123 . hal-03773720

HAL Id: hal-03773720

<https://hal.science/hal-03773720>

Submitted on 9 Nov 2022

HAL is a multi-disciplinary open access archive for the deposit and dissemination of scientific research documents, whether they are published or not. The documents may come from teaching and research institutions in France or abroad, or from public or private research centers.

L'archive ouverte pluridisciplinaire **HAL**, est destinée au dépôt et à la diffusion de documents scientifiques de niveau recherche, publiés ou non, émanant des établissements d'enseignement et de recherche français ou étrangers, des laboratoires publics ou privés.

Evaluation of LIF thermometry technique using Krypton as a tracer: Impact of laser lineshape and collisional bandwidth

Nathalie Lamoureux^a, Pradeep Parajuli^b, Waruna Kulatilaka^b, Pascale Desgroux^{a,*}

^a Univ. Lille, CNRS, UMR 8522 - PC2A - Physicochimie des Processus de Combustion et de l'Atmosphère, F-59000 Lille, France

^b J. Mike Walker '66 Department of Mechanical Engineering, Texas A&M University, College Station, TX 77843, USA

Abstract

In recent years, two-photon laser-induced fluorescence (TPLIF) of inert gas krypton (Kr) has received much attention as a potential non-intrusive flow diagnostics, thermometry, and velocimetry technique. However, the interaction between the laser bandwidth and the atomic excitation transition at varying pressures, and losses of fluorescence quantum efficiency due to spatially varying collisional quenching of Kr are not fully understood. The resulting lineshape and quenching corrections become especially important when the temporal scales of excitation laser pulses vary from nanosecond (ns) to femtosecond (fs) timescales. In this study, we report a comprehensive investigation of Kr line broadening and quenching effects, in particular, with respect to TPLIF-based temperature (T) measurements in flames. Experiments were conducted in both low-pressure and atmospheric-pressure flames and in two different burner configurations, using conventional ns and ultrafast fs duration laser sources. When using ns pulses, the results suggest no lineshape corrections are necessary at low pressure; however, a T -dependent empirical model was needed for atmospheric-pressure flames. In contrast, broadband fs pulses have linewidths in excess of 400 cm^{-1} , which are significantly larger than sub-cm^{-1} spectral transitions, hence requiring no lineshape corrections at any pressure. A quenching rate model which scales as $T^{-0.5}$ was developed and validated using previous low-pressure thermometry data and 1D flame model predictions. The Kr TPLIF temperature profiles measured using ns pulses (low and atmospheric pressures) and fs pulses (atmospheric pressures) agreed well with model predictions. In the absence of the necessity for lineshape corrections, fs Kr-TPLIF provides an easy way to extract T simply by taking the inverse square of the fluorescence signal. Fs T line imaging results are presented for several flame heights. The present study establishes a simplified approach for Kr TPLIF-based thermometry in flames.

Keywords: LIF Thermometry; Krypton; Two-Photon LIF; Nanosecond Excitation; Femtosecond Excitation; Linewidth Effects

*Corresponding author.

1 Introduction

Temperature (T) is of major interest in characterizing flames and combustion systems. Laser-based techniques offer the advantage of non-intrusive measurements with high spatial and temporal resolution. The most widely used laser-based thermometry techniques for gas temperature are based on Rayleigh scattering, Raman and Coherent Anti-Stokes Raman scattering (CARS), absorption spectroscopy, and laser-induced fluorescence (LIF) [1–5].

A number of these techniques are based on the direct proportionality between the collected signal and the total density (i.e., Rayleigh scattering) or the density of an individual species (i.e., Raman scattering). Thus, Rayleigh scattering has long been employed due to its apparent simplicity and to its applicability (1D or 2D) in a wide range of combustion configurations [6]. This technique depends on the elastic scattering from the species present locally in the mixture. The Rayleigh intensity is proportional to the sum of the densities of each species multiplied by their scattering cross-sections. The temperature is determined from the deduced local number density. Despite numerous advantages and applications, this technique suffers from possible spectral interferences and variation of the total scattering cross-section due to changes in the composition of the probed volume. On the contrary, data reduction from the inelastic Raman scattering techniques is more direct since the Raman signal is species-selective, besides the signal being very weak. Raman and Rayleigh techniques have led to many imaging applications (see, for instance, [6,7]), but these techniques are typically restricted to fields without particles.

Recently Zelenak and Narayanaswamy [3] proposed a thermometry approach based on the two-photon LIF (TPLIF) of krypton (Kr) seeded upstream into the reacting flow. Krypton has been used as a tracer species in several applications; using X-ray fluorescence for the probe perturbation analysis [8], for thermometry [9], and using TPLIF of krypton to measure the mixture fraction in flames [10] or for high-speed flow diagnostics [11,12]. The thermometry technique in Ref [3] took advantage of the spectral line broadening with temperature. The Kr linewidth, which is the convolution between the laser and the absorption lineshape (the latter being T dependent), was determined by scanning over the $5p^3P_2 \leftarrow 4p^6^1S_0$ transition of Kr. The excitation wavelength of the nanosecond (ns) pulsed laser was around 214 nm with a pulse duration of approx. 7-ns and a spectral bandwidth of 0.06 cm^{-1} , fullwidth-at-half-maximum (FWHM). The fluorescence signal was collected at 760 nm.

After applying a deconvolution procedure, they could extract either the Doppler broadening or the collisional broadening of the Kr excitation transition. The temperature is then deduced from these

linewidths, which were pre-calibrated as a function of T . This calibration was based on a complex and extensive procedure to independently measure T by Rayleigh scattering over a wide range of gas compositions and temperatures. Measurements were performed in an atmospheric-pressure laminar methane diffusion flame. The uncertainty was estimated to be 109 K in the “core” and 73 K in the flame zone. A two-line variant of this approach [13] was then applied to measure T in sooting diffusion flames [14].

It turns out that Zelenak and Narayanaswamy [3] took advantage of the narrow linewidth of their excitation laser as compared with the absorption lineshape. However, this condition is difficult to satisfy in many commercial pulsed laser systems.

On the other hand, it may be possible to measure T using the attractive TPLIF of Kr method, but by simply following its density. Similar to Rayleigh thermometry, seeded Kr density in the flame is nearly proportional to $1/T$. It is to be noted that the density of Kr in a helicon plasma was previously determined by TPLIF [15]. Among the possible Kr transitions from the ground state, we propose the $5p^1D_2$ ($2 \times 204\text{ nm}$) to take advantage of the proximity to the H-atom line for further detection by TPLIF [16,17]

Hence the objective of this work is to evaluate the performance of TPLIF thermometry based on Kr density by analyzing both the effect of laser lineshape and collisional bandwidth. The first aspect was achieved by using a ns-laser (0.2 cm^{-1} FWHM) and a femtosecond (fs) laser (bandwidth of approx. 430 cm^{-1}). Note that the excessive bandwidth of the fs-laser can indeed be advantageous for efficient two-photon excitation of narrow atomic transitions [18]. The collisional bandwidth impact was examined by studying premixed $\text{CH}_4/\text{O}_2/\text{N}_2$ flames at different pressures: low-pressure flat flames (5.3 and 10.6 kPa) and atmospheric-pressure Bunsen flames. The temperatures determined by Kr TPLIF are compared to previous measurements obtained by LIF thermometry of NO or OH in the low-pressure flames and equilibrium calculations in the Bunsen flames assuming adiabatic conditions. In each flame, the quenching rate is evaluated either from the temporal LIF signal decay or by using literature collisional cross-sections.

The rest of the paper is organized as follows. Section 2 presents the experimental details of the burners and the excitation/detection systems using a ns laser system at University of Lille (ULille) and a fs-laser system at Texas A&M University (TAMU). Section 3 outlines the related theory for estimating spectral lineshape profile and collisional quenching. Results and discussion from the low-pressure flames (ns-excitation) and atmospheric-pressure flames (both ns and fs excitations) work are presented in Sections 4 & 5, respectively, followed by some concluding remarks in Section 6.

2 Experimental set-up

2.1 Burners

Experiments were undertaken in laminar methane flames stabilized either at low pressure on a 6-cm diameter bronze water-cooled McKenna burner (B1) or at atmospheric pressure in 13 mm-diameter (ID) Bunsen burners (B2 at ULille, B3 at TAMU). Details about the burners and the gas supply are given in Ref. [17,4,19] for B1, B2, and B3, respectively. At low pressure, three flames were selected (F1, F2, F3) because the temperature profiles as a function of height-above-the-burner (HAB) have previously been measured using LIF thermometry (OH or NO) [20–22] and will serve as reference T profiles. Atmospheric-pressure Bunsen flames were selected because the temperature at the flame front and in the vicinity of the reaction zone can be assumed adiabatic, and the T profiles as a function of radial distance can be calculated using one-dimensional (1-D) simulation codes. The volumetric gas flow rates of the studied flames metered using mass flow controllers (MFC) are reported in Table 1. Krypton gas (Air Products, purity 99.999%) used as a tracer was introduced to the mixture gas line.

Table 1
Flame compositions. Gas flow rates are reported in slpm (at 273.15 K and 101.3 kPa). ϕ is the equivalence ratio.

Flame	p (kPa)	CH ₄	O ₂	N ₂ +Kr	ϕ
F1	5.33	0.60	0.96	3.29	1.25
F2	5.33	0.48	0.96	3.35	1.00
F3	10.66	0.48	0.96	3.35	1.00
F4	atm	0.857	1.718	6.463	1.00
F5	atm	0.775	1.55	5.858	1.00

2.2 Laser systems

At ULille, the pulsed laser system consisted of an approx. 7-ns-duration (FWHM) frequency-doubled Nd:YAG laser (Continuum, Powerlite DLS8000) pumping a dye laser (Continuum, ND6000) providing radiation at 615 nm, with a repetition rate of 10 Hz. The fundamental frequency of the dye laser was doubled using a KDP crystal. The doubled and the residual fundamental beams were then mixed in a BBO crystal to generate 205-nm radiation. The laser bandwidth of the doubled dye laser output was determined to be 0.16 cm^{-1} at 305 nm from previous work, and the 204.13-nm bandwidth is estimated to be around $0.15\text{--}0.2 \text{ cm}^{-1}$. The experimental set-up is identical to the one described in [17], except that a fast photomultiplier tube (PMT) (Hamamatsu, H11625-20-NF, 0.5 ns rise time) was used. Each measurement represents an accumulation of 600 laser shots, and profiles along HAB or radial distance (r) were repeated at least three times. With burner B1, half of one of the collection lens was blocked in order to prevent additional correction of the variation of the solid angle of collection. This variation was found

negligible with the burner B2 and, the lens was unblocked in order to increase the collected signal.

The fs-laser system at TAMU consists of a frequency-tunable, regeneratively amplified 1-kHz Ti:Sapphire laser (Spectra Physics, Solstice Ace). The ~ 80 -fs-duration (FWHM) fundamental output near 820 nm was used to pump a custom-built fourth harmonic generator (FHG) unit to obtain deep ultraviolet (DUV) radiation centered at 204.1 nm [16]. The DUV output beam was guided through several dielectric laser mirrors and focused onto the probe region using a +500-mm focal length lens. Kr-TPLIF line images were recorded orthogonal to the laser beam direction using an intensified charge-coupled device (ICCD) camera (Princeton Instruments, PIMax IV). The ICCD camera was fitted with a 50-mm focal length $f/1.2$ Nikon visible camera lens and a bandpass filter (Semrock, FF01-832/37-50). The intensifier gate width was set to 10 ns, and a gain of 100% was used. In a typical experiment, 100 laser shots were accumulated on the camera, and 100 such images were averaged and recorded at each flame height. The laser energy was held fixed at $3.5 \pm 0.05 \mu\text{J/pulse}$ to avoid ionization and amplified spontaneous emission (ASE). Kr emission spectrum was also monitored in the 750–840 nm range by using a spectrometer/camera combination (Princeton Instruments Isoplan160)/PIMax IV) to ensure the signal collected through the filter bandwidth consisted of only Kr emission peaks [11]. Interference due to the fundamental laser wavelength at 820 nm was removed during data processing by subtracting a background image.

For both experimental schemes, the absence of ASE was checked, and measurements were performed in the quadratic regime of LIF. Flames were seeded with 0.4%, 1%, and 5% Kr substituted for N₂, respectively, for flames F1-F3, F4 and F5.

3 Theory

Krypton is excited from the ground state $4p^6 \text{ } ^1\text{S}_0$ to the excited level $5p^5 \text{ } ^1\text{D}_2$ at 97945.16 cm^{-1} via a two-photon absorption at 204.13 nm. For ns experiments, the TPLIF signal is collected at 826.5 nm from the $5p^5 \text{ } ^1\text{D}_2 \rightarrow 5s^5 \text{ } ^1\text{P}_1$ transition. To improve the quality of line imaging experiments, the signals collected in fs experiments include all 5p to 5s emission transitions at 760, 786, 811, and 826 nm [11].

According to Refs [17,23], the time-integrated TPLIF signal of Kr, S_{Kr} , that is T -dependent, can be expressed as a function of the Kr density [Kr] as follows:

$$S_{Kr} \propto \mathcal{g}(\Delta\bar{\nu}) \frac{A_{32}}{A_3 + Q_{Kr}} [\text{Kr}] (I_\nu)^2 \quad (1).$$

Here $\mathcal{g}(\Delta\bar{\nu})$ is the normalized line profile of the two-photon excitation, which is composed of the convolution of the effective laser line profile and the atomic absorption line. A_3 is the total spontaneous

emission rate of the $n = 3$ excited level, A_{32} is the spontaneous emission rate along $3 \rightarrow 2$. Q_{Kr} is the total quenching rate. $A_3 + Q_{Kr}$ is the total depopulation rate of the upper level or the fluorescence decay rate. I_v is the laser intensity at the wavenumber $\bar{\nu}$. To extract the temperature, we need to consider the T dependence of Q_{Kr} , $g(\Delta\bar{\nu})$ and $[Kr]$. In isobaric flows, $[Kr]$ scales as X_{Kr}/T , where X_{Kr} is the Kr mole fraction. Hence, Eq (1) becomes:

$$S_{Kr} \propto g(\Delta\bar{\nu}) \frac{A_{32} X_{Kr}}{A_3 + Q_{Kr} T} (I_v)^2 \quad (2)$$

X_{Kr} is equal to the ratio of the Kr mole number to the total mole number, which can vary along HAB. This latter is calculated using ‘‘Premixed laminar flame’’ of Chemkin-Pro software [24] and its variation was taken into account in the flames investigated in this work (See SM-1).

The *Quenching rate* can be evaluated from three different methods. The first is from the fluorescence decay, particularly if it is sufficiently long in comparison to the excitation laser pulse. Such can be achievable in low-pressure flames with a fast response time PMT (~ 0.5 ns) and ns laser. The second method is using the collisional cross-sections of Kr reported in the literature. Niemi et al. [25] reported data for the reactant colliders in the level $5p^1D_2$, and Hsu et al. [10] reported data for the main colliders except for CO but for the level $5p^3P_2$. This correction further requires the knowledge of the flame composition at any location, which can be determined from flame modeling. In the third approach, it can be estimated from the assumption of a $T^{0.5}$ dependence of Q_{Kr} along the flame. These three approaches are examined in the present study as detailed in Section 4.1.

The *lineshape profile* $g(\Delta\bar{\nu})$ which depends on the Doppler, collision, and laser broadenings is estimated by scanning the ns excitation laser over the absorption line at different T and p . No widening was observed neither at low pressure with the ns-laser ($\Delta\nu_c \sim 0$) nor at atmospheric pressure with the fs-laser ($\Delta\nu_l \gg \Delta\nu_{abs}$). But with the ns-laser at atmospheric pressure, the widening of the normalized lineshape profile is visible with the decrease of T and could be fitted by:

$$g(\Delta\bar{\nu}) = 1.985 \times 10^{-4} \times T / K + 0.580 \quad (3)$$

with $g(\Delta\bar{\nu}) = 1$ in the hot gases ($T=2116K$).

4 Results from the low-pressure flames

The fluorescence decay is long enough to allow the measurement of the quenching rate profile using the ns-system in low-pressure flames (F1–F3). The complete procedure is detailed hereafter in flame F1, for which different thermometry methods have already been applied to determine the temperature profiles (NO-LIF, OH-LIF, and thermocouple) [20]. The probe volume in burner B1 was estimated to be

$6.0 \times 0.2 \text{ mm}^2$ parallel to the burner surface and $250 \text{ }\mu\text{m}$ in the vertical axis.

4.1 Quenching rate

The LIF decay rate is extracted using a deconvolution method described in [17]. Rayleigh scattering signal at 615 nm was measured with the PMT used during this work. Additional Stern-Volmer plots of Kr highly diluted in N_2 were measured from 1 to 15 kPa in a cell at room T . The results indicate the fluorescence decay rate follows a linear increase with p up to $4 \times 10^8 \text{ s}^{-1}$ (i.e. $\tau = 2.5$ ns) with a quenching rate identical to the one given in [25]. Since the quenching coefficients reported in [25] for the level $5p^1D_2$ are incomplete, we chose to use the complete data reported in [10] for the main colliders even though they correspond to the excited level $5p^3P_2$. The cross-section of CO was taken equal to that of CO_2 .

In flames, Q_{Kr} along HAB were also calculated using simulated species profiles, the collisional cross-sections from [10] and the temperature profile previously measured using OH-LIF thermometry [20]. As shown in Fig. 1, the experimental Q_{Kr} as a function of HAB is found to be in very good agreement with the calculated values for $HAB > 3.2$ mm. Below this height, i.e., in the low-temperature region, experimental Q_{Kr} are found 20% larger probably because they exceed the limit above-mentioned of $4 \times 10^8 \text{ s}^{-1}$. Below this limit, the good agreement between experimental and calculated Q_{Kr} gives confidence in the further use of these collisional cross-sections at atmospheric pressure (indeed, Q_{Kr} is expected to reach $8 \times 10^9 \text{ s}^{-1}$ and is therefore difficult to measure). In addition, as shown by the dashed line in Fig. 1, it is also observed that Q_{Kr} scales according to $T^{0.5}$ [26]. Since A_3 is negligible ($2.9 \times 10^7 \text{ s}^{-1}$, [25]) compared to Q_{Kr} , the total depopulation rate ($A_3 + Q_{Kr}$) can hence be assumed to vary as $T^{0.5}$. The uncertainty in determining Q_{Kr} is estimated to be 20% (absolute value) but only 2.5% for the relative variation of Q_{Kr} .

4.2 Time-integrated LIF measurements

The time-integrated fluorescence signal of Kr, S_{Kr} , corrected for the square of the laser intensity fluctuations I_v was obtained as a function of HAB. At low pressure, the lineshape profile was found constant along the HAB, hence was not considered. Knowing the experimental ($A_3 + Q_{Kr}$), the relative temperature is determined according to Eq. (2). Then, the relative T profile is converted into absolute T using the calibration point at $HAB=20$ mm from previous OH-LIF thermometry measurements [20]. Figure 2 shows the temperature profile obtained in flame F1 using different techniques. We observe a near-perfect agreement with the temperature profiles previously determined using NO-LIF, OH-LIF thermometry. As the OH-LIF thermometry method is restricted to locations where OH radicals are naturally formed, the profile was completed in the fresh zone using a thin commercial thermocouple (type K). Here, the Kr TPLIF thermometry allows describing the full profile.

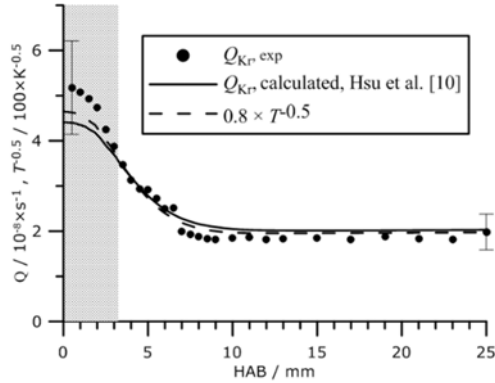


Fig. 1. Measured (solid circles) and calculated (solid line) quenching rates as functions of HAB in flame F1. Also shown is the variation of $T^{-0.5}$ (dash line), scaled by 0.8 for easy comparison. The error bar indicates the total experimental uncertainty (20%) on Q_{Kr} .

Temperature profiles similarly measured in flames F2 and F3 also show a very good agreement with the T profiles previously measured using NO-LIF thermometry in [21,22], see SM-2.

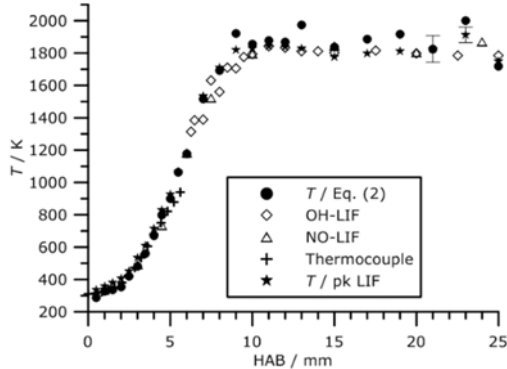


Fig. 2. Temperature profile as a function of HAB measured from the Kr TPLIF signal in flame F1.

4.3 Prompt-LIF (temporal peak)

In section 4.2, the correction for Q_{Kr} variation required a separate record of the fluorescence temporal trace at each location. We have also examined the possibility to determine the T profile directly from the inverse of the prompt-LIF measurements, i.e., without quenching correction. Prompt LIF is defined as the temporal peak value of LIF (pk LIF). Figure 2 shows that temperature profiles determined either from pk LIF or from Eq. (2) are also in good agreement. The experimental uncertainties are estimated to be equal to 5% when T is derived from Eq. (2) (including 2.5% due to the determination of Q_{Kr}) and 2.5% when T is derived from the pk LIF signal as shown in Fig. 2.

To conclude about the thermometry measurements performed in low-pressure flames, it appears that the

prompt-LIF is not affected by the quenching, unlike the integrated LIF, which must be corrected for its spatial variation. And, this method allows temperature measurements provided that there is a reference temperature along the profile either in the burned gas or in the fresh gas.

5 Results from the atmospheric-pressure flames

At atmospheric pressure, it is expected that the prompt-LIF signal will indubitably be affected by the fast quenching rates, especially when excitation is performed with a ns-laser. Hence, experiments in similar atmospheric-pressure Bunsen burners were performed using a ns-laser and a fs-laser at ULille and TAMU, respectively. In these flames, the TPLIF thermometry of Kr is described along the radial axis at different HAB's. In these 13-mm exit diameter Bunsen flames, T is expected to be nearly uniform and estimated to be at the adiabatic flame temperature of 2115 K (and 2135 K) in the region of $5 < r / \text{mm} < 8$, in flames F4 (and F5). Beyond approx. $r = 8$ mm, T drops rapidly because of the diminishing reaction zone and rapid mixing with outside cold air in the outer shear layer. Outside air mixing also result in X_{Kr} drop.

As the determination of T from Eq. (2) is not direct (Q is not measurable), we propose to compare the experimental and the synthetic S_{Kr} profiles instead of the derived quantities (here T profiles). This approach follows the paradigm shift proposed by Connelly et al. [27] who argued that the comparison of the signals involves less data and is more straightforward. Here the main difficulty lies in the determination of both the quenching rate and the lineshape, which requires an estimation of the T profile to start with. First, the temperature and species profiles have been calculated along the normal axis of the flame front using Chemkin-Pro software for a freely propagating flame. This method allows the calculation of Q_{Kr} and X_{Kr} . Note that the calculated Q_{Kr} along the flame axis was found to evolve quite similarly to $T^{-0.5}$ as in low-pressure flames (see SM-3). The simulated values are projected on the radial axis knowing the angle of the flame front, and $g(\Delta\vec{v})$ is calculated according to Eq. (3) for ns-TPLIF. Subsequently, the temperature is determined from the experimental TPLIF profiles, corrected as detailed below, and using a known T .

5.1 Using ns-duration laser pulses

Kr TPLIF measurements were performed along the radial axis at 7 mm above the burner exit, first using a ns-laser at ULille. The probe volume in burner B2 was carefully restricted to allow an adequate spatial resolution along the steep gradient of T in the flame front. It is estimated to be $200 \times 200 \mu\text{m}^2$ parallel to the burner tip and $250 \mu\text{m}$ in the vertical axis. Figure 3 shows the comparison between the experimental LIF profile along the radial axis and the synthetic LIF signal obtained from the simulated T and X_{Kr} profiles

and corrected for the lineshape broadening and the quenching rate according to Eq. (2). The ratio of the LIF signals between the cold and the hot area is approximately a factor of 2 (right side), while the ratio of T^{-1} is approx. 7 (grey line in the left). On the left, indicated are the successive corrections applied to the calculated T^{-1} for (a) the variation of the total mole number X_{Kr} (dot-dashed line), (b) the lineshape profile $g(\Delta\bar{\nu})$ (dashed line), and (c) the total depopulation rate (A_3+Q_{Kr}) (solid line). The correction factor for the variation of the mole fraction is nearly equal to 1 while those for $g(\Delta\bar{\nu})$ and A_3+Q_{Kr} , are equal to 0.65 and 0.40, respectively. Finally, the ratio of the synthetic LIF signals between the cold and the hot area is equal to 2. This ratio is in agreement with the experimental LIF ratio shown on the right side of Fig. 3 (which is simply a magnification of the grey area on the left). These observations give confidence that the same corrections could be applied to obtain the relative T profile from the Kr TPLIF signals, as discussed below.

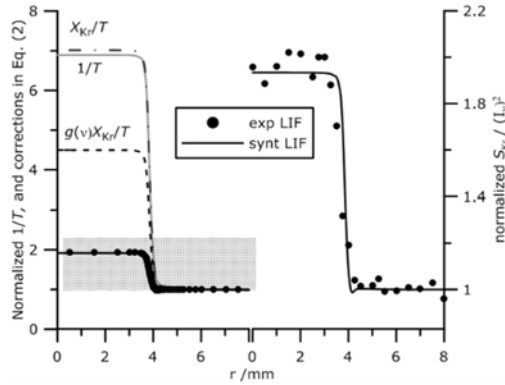


Fig. 3. Comparison of the experimental and synthetic LIF signal at 7 mm using a ns-laser in a Bunsen burner. The left side shows the variation of the inverse of T , and the successive corrections applied to T^{-1} to calculate a LIF signal according to Eq. (2). The right side is a magnification of the grey area on the left.

Using an iterative procedure including the corrections for Q_{Kr} scaled as $T^{-0.5}$ and $g(\Delta\bar{\nu})$, the temperature profile was determined from the Kr TPLIF, calibrated using the hot temperature of 2115 K. Figure 4 (left side) shows a good agreement between the experimental and the simulated temperature profiles obtained in Bunsen burner B2 using ns Kr-TPLIF. In particular, the steepness of the gradient is well reproduced and the deduced cold T is 287 K i.e. 4% lower than the temperature measured by thermocouple on the burner axis.

5.2 Using fs-duration laser pulses

Similarly, Kr TPLIF measurements were performed along the radial axis at three HAB locations using the fs-laser at TAMU. The raw fluorescence images recorded by seeding 5% Kr into

F5 flame are shown in Fig. 5. The typical width of the line filled about 8 pixels in the camera plane, corresponding to a spatially calibrated beam waist of 0.220 mm. The typical signal-to-background ratio in the inner premixed reactants zone is approx. 13, and that in the hot flame zone is 7. Those values changed to 5 and 3, respectively, when the Kr seeding level was changed to 1%. However, the general profile shapes remained unchanged. The signal-to-noise ratio (SNR) values defined as the mean signal divided by one standard deviation are approximately 4.5 and 6 for 5% and 1% seeding levels, respectively.

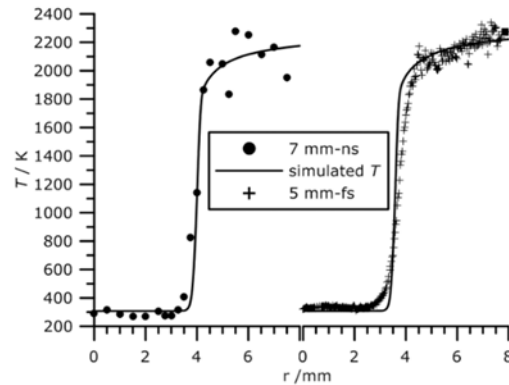


Fig. 4. Comparison between the simulated and experimental T profiles determined from the Kr-LIF signal measured with a ns-laser at 7 mm (left) or with a fs-laser at 5 mm (right).

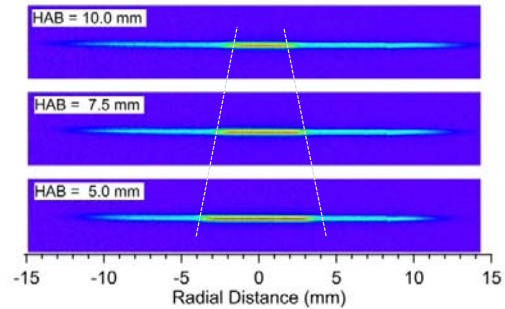


Fig. 5. fs TPLIF line images in F5 recorded at three different HAB locations.

Figure 6 shows the corresponding LIF signals obtained by vertically integrating the line images shown in Fig. 5. Only the right half of the nearly-perfectly symmetric line profiles are shown. The relative signals are normalized to the values of $5 < r / \text{mm} < 8$ region. The ratio between the cold and the hot area of the LIF signal is equal to approx. 2.5, slightly higher than the ratio observed with a ns-laser in F4.

The conversion of the fs TPLIF signal into temperature profile requires only the knowledge of the quenching rate along the radial axis. Since the bandwidth of the fs laser is so large, the variation in

$g(\Delta\bar{\nu})$ across the flame can easily be neglected. Hence, assuming a $T^{-0.5}$ dependence of Q_{Kr} and neglecting the variation of X_{Kr} , Eq. (2) simplifies to:

$$S_{Kr} \propto (T)^{-0.5}(I_V)^2 \quad (4)$$

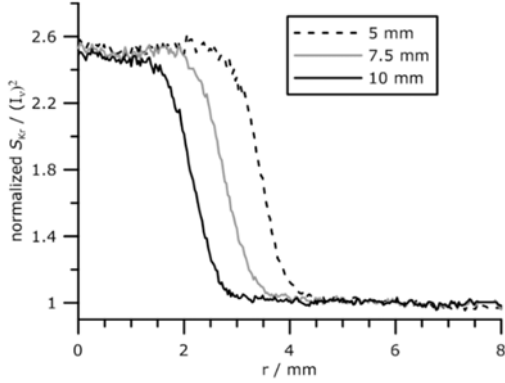


Fig. 6. Normalized LIF signals along the radial axis measured at HAB = 5, 7.5, and 10 mm with a fs-laser.

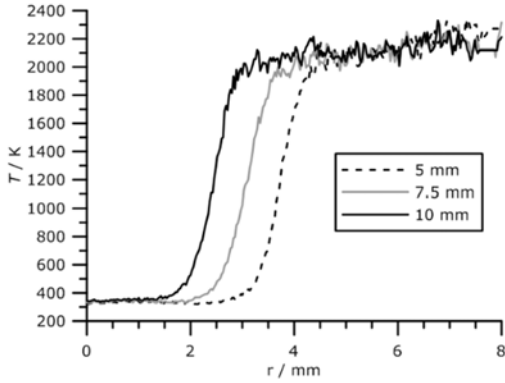


Fig. 7. Radial T profiles obtained using fs-TPLIF in F5 at HAB = 5, 7.5, and 10 mm using the calibration procedure outlined in Eq. (4).

Hence, fs TPLIF returns an easy way to extract the temperature simply from the inverse square of the fluorescence signal (provided the excitation laser intensity is held fixed). This method has been applied to the Kr TPLIF line images recorded with the fs-laser at TAMU. The conversion to the absolute temperature was performed using a calibration point where the hot area of the flame is assumed to be at the adiabatic temperature of 2135 K. Accordingly, the radial TPLIF signals profiles shown in Fig. 6 are converted to the corresponding T profiles using Eq. 4 and are shown in Fig. 7. Again, for better clarity, only the right half of the nearly perfectly symmetric radial T profiles are shown. The T profile measured at HAB = 5 mm is also reproduced in Fig. 4 (right side) and compared with modeling. Again, the increase in T ($\times 7$) between the burner axis and the burnt gases is very well reproduced. The advantage of the fs-approach over

that of ns is clearly the simpler conversion of the TPLIF signal to temperature using Eq. (4). The accuracy is estimated at 5% over the entire T range.

6 Conclusions

In this study, we report a comprehensive investigation of LIF-based thermometry in flames using Kr as an inert gas tracer. Two of the major obstacles for quantitative LIF measurements are, i) interaction between the laser bandwidth and the broadening of atomic excitation transition, necessitating spectral overlap corrections, and ii) the effect of spatially varying non-radiative decay of the excited state population due to collisional quenching. We investigate narrowband ns-duration as well as broadband fs-duration excitation pulses for Kr TPLIF thermometry. When using ns pulses, no lineshape correction was needed in low-pressure flames; however, atmospheric pressure flames required a lineshape correction based on a T -dependent empirical model. In contrast, fs pulses have linewidths in excess of $\sim 400 \text{ cm}^{-1}$, hence, do not require any spectral overlap correction with varying pressures.

In the low-pressure premixed flames investigated, the experimentally measured quenching rates Q_{Kr} agree satisfactorily with those calculated using quenching cross-sections reported in the literature and simulated species mole fractions. It is also shown that the experimental Q_{Kr} scales as $T^{-0.5}$. The flame temperatures, estimated after correction for the T dependence of Q_{Kr} , agree well with previously reported NO and OH LIF thermometry data, as well as those estimated using prompt-LIF without any quenching corrections. The uncertainty using prompt-LIF is estimated to be 2.5%. In the atmospheric-pressure flames, the ns experimental Kr fluorescence signals could be fitted well using an iterative procedure using calculated Q_{Kr} , T^{-1} number density dependence, and empirical lineshape profile model. The extracted radial T profiles in a Bunsen-type flame agree well with simulated 1D temperature profiles using Chemkin-Pro.

In contrast, the conversion of the fs TPLIF signal into temperature profile requires only the knowledge of the quenching rate, which can be approximated by $T^{-0.5}$ dependence. Hence, fs TPLIF provides an easy way to extract the flame temperature, with an accuracy estimated at 5%, simply by taking the inverse square of the fluorescence signal. Accordingly, fs-TPLIF line images were recorded at several HAB locations in the Bunsen flame and converted to radial T profiles. It was confirmed these T profiles agree well with 1D flame model predictions. Therefore, fs-TPLIF is a promising approach for thermometry in atmospheric and higher-pressure flames. In addition, nearly impulsive excitation using fs-duration pulses provides a means of measuring species-specific quenching rates of Kr at atmospheric and elevated pressures, which will be a topic for future investigation.

Acknowledgements

This work is a contribution to the CPER research project CLIMIBIO. PD and NL thank the MESR, the Hauts-de-France Region and the ERDF for their financial support and the CORIA for providing the Bunsen burner. PP and WK acknowledge funding support from the US National Science Foundation (NSF) (Contract No. CBET- 1604633).

Supplementary material

SM.pdf file is provided.

References

- [1] N.M. Laurendeau, Temperature measurements by light-scattering methods, *Prog. Energy Combust. Sci.* 14 (1988) 147–170.
- [2] S. Roy, J.R. Gord, A.K. Patnaik, Recent advances in coherent anti-Stokes Raman scattering spectroscopy: Fundamental developments and applications in reacting flows, *Prog. Energy Combust. Sci.* 36 (2010) 280–306.
- [3] D. Zelenak, V. Narayanaswamy, Composition-independent mean temperature measurements in laminar diffusion flames using spectral lineshape information, *Exp. Fluids.* 58 (2017) 147.
- [4] K.K. Foo, N. Lamoureux, A. Cessou, C. Lacour, P. Desgroux, The accuracy and precision of multi-line NO-LIF thermometry in a wide range of pressures and temperatures, *J. Quant. Spectrosc. Radiat. Transfer.* 255 (2020) 107257.
- [5] C.S. Goldenstein, R.M. Spearrin, J.B. Jeffries, R.K. Hanson, Wavelength-modulation spectroscopy near 2.5 μm for H₂O and temperature in high-pressure and -temperature gases, *Appl. Phys. B.* 116 (2014) 705–716.
- [6] F.-Q. Zhao, H. Hiroyasu, The applications of laser Rayleigh scattering to combustion diagnostics, *Prog. Energy Combust. Sci.* 19 (1993) 447–485.
- [7] A. Lo, F. Frat, E. Domingues, A. Lacour, B. Lecordier, P. Vervisch, A. Cessou, Nanosecond pulsed discharge in a propane–air mixture: Ignition and energy deposition, *Proc. Combust. Inst.* 36 (2017) 4087–4094.
- [8] N. Hansen, R.S. Tranter, K. Moshhammer, J.B. Randazzo, J.P.A. Lockhart, P.G. Fugazzi, T. Tao, A.L. Kastengren, 2D-imaging of sampling-probe perturbations in laminar premixed flames using Kr X-ray fluorescence, *Combust. Flame.* 181 (2017) 214–224.
- [9] E. Boigné, N.R. Bennett, A. Wang, K. Mohri, M. Ihme, Simultaneous in-situ measurements of gas temperature and pyrolysis of biomass smoldering via X-ray computed tomography, *Proc. Combust. Inst.* 38 (2021) 3899–3907.
- [10] A.G. Hsu, V. Narayanaswamy, N.T. Clemens, J.H. Frank, Mixture fraction imaging in turbulent non-premixed flames with two-photon LIF of krypton, *Proc. Combust. Inst.* 33 (2011) 759–766.
- [11] Y. Wang, C. Capps, W.D. Kulatilaka, Femtosecond two-photon laser-induced fluorescence of krypton for high-speed flow imaging, *Opt. Lett.* 42 (2017) 711–714.
- [12] D. Shekhtman, M.A. Mustafa, N.J. Parziale, Two-photon cross-section calculations for krypton in the 190–220 nm range, *Appl. Opt.* 59 (2020) 10826–10837.
- [13] D. Zelenak, V. Narayanaswamy, Demonstration of a two-line Kr PLIF thermometry technique for gaseous combustion applications, *Opt. Lett.* 44 (2019) 367–370.
- [14] A. Sahoo, V. Narayanaswamy, Two-dimensional temperature field imaging in laminar sooting flames using a two-line Kr PLIF approach, *Appl. Phys. B.* 125 (2019) 168.
- [15] R.M. Magee, M.E. Galante, D. McCarren, E.E. Scime, R.L. Boivin, N.H. Brooks, R.J. Groebner, D.N. Hill, G.D. Porter, A two photon absorption laser induced fluorescence diagnostic for fusion plasmas, *Rev. Sci. Instrum.* 83 (2012) 10D701.
- [16] W.D. Kulatilaka, J.R. Gord, S. Roy, Femtosecond two-photon LIF imaging of atomic species using a frequency-quadrupled Ti:sapphire laser, *Appl. Phys. B.* 116 (2014) 7–13.
- [17] N. Lamoureux, K.K. Foo, P. Desgroux, Quantitative measurement of atomic hydrogen in low-pressure methane flames using two-photon LIF calibrated by krypton, *Combust. Flame.* 224 (2021) 248–259.
- [18] W.D. Kulatilaka, J.R. Gord, V.R. Katta, S. Roy, Photolytic-interference-free, femtosecond two-photon fluorescence imaging of atomic hydrogen, *Opt. Lett.* 37 (2012) 3051–3053.
- [19] A. Jain, Y. Wang, W.D. Kulatilaka, Effect of H-atom concentration on soot formation in premixed ethylene/air flames, *Proc. Combust. Inst.* 37 (2019) 1289–1296.
- [20] N. Lamoureux, P. Desgroux, A. El Bakali, J.F. Pauwels, Experimental and numerical study of the role of NCN in prompt-NO formation in low-pressure CH₄/O₂/N₂ and C₂H₂/O₂/N₂ flames, *Combust. Flame.* 157 (2010) 1929–1941.
- [21] N. Lamoureux, H. El Merhubi, L. Pillier, S. de Persis, P. Desgroux, Modeling of NO formation in low pressure premixed flames, *Combust. Flame.* 163 (2016) 557–575.
- [22] N. Lamoureux, P. Desgroux, In Situ Laser-Induced Fluorescence and Ex Situ Cavity Ring-Down Spectroscopy Applied to NO Measurement in Flames: Microprobe Perturbation and Absolute Quantification, *Energy Fuels.* 35 (2021) 7107–7120.
- [23] A. Goehlich, T. Kawetzki, H.F. Döbele, On absolute calibration with xenon of laser diagnostic methods based on two-photon absorption, *J. Chem. Phys.* 108 (1998) 9362–9370.
- [24] Chemkin-Pro, ANSYS, Inc., Canonsburg, PA, 2021.
- [25] K. Niemi, V. Schulz von der Gathen, H.F. Döbele, Absolute atomic oxygen density measurements by two-photon absorption laser-induced fluorescence spectroscopy in an RF-excited atmospheric pressure plasma jet, *Plasma Sources Sci. Technol.* 14 (2005) 375–386.
- [26] W.D. Kulatilaka, J.H. Frank, T.B. Settersten, Interference-free two-photon LIF imaging of atomic hydrogen in flames using picosecond excitation, *Proc. Combust. Inst.* 32 (2009) 955–962.
- [27] B.C. Connelly, B.A.V. Bennett, M.D. Smooke, M.B. Long, A paradigm shift in the interaction of experiments and computations in combustion research, *Proc. Combust. Inst.* 32 (2009) 879–886.

Supplementary Materials to “Evaluation of LIF thermometry technique using Krypton as a tracer: Impact of laser lineshape and collisional bandwidth”

Nathalie Lamoureux^a, Pradeep
Parajuli^b, Waruna Kulatilaka^b,
Pascale Desgroux^{a,*}

DOI:

1/ Variation of the calculated mole fraction of Kr in the investigated flames

In low-pressure flames (F1-F3), the temperature profiles were previously measured using OH, NO LIF thermometry and thermocouple as explained in Lamoureux et al. [1–3]. The variation of the total mole number is calculated using the “burner stabilized flame module” of Chemkin-Pro [4]. The atmospheric flames are assumed to be adiabatic, and the simulated variation of the total mole number along the radial axis was calculated using the “flame speed module” of Chemkin-Pro. For clarity, the results are presented in Figs. S1 and S2 for the low-pressure and the atmospheric pressure flames, respectively.

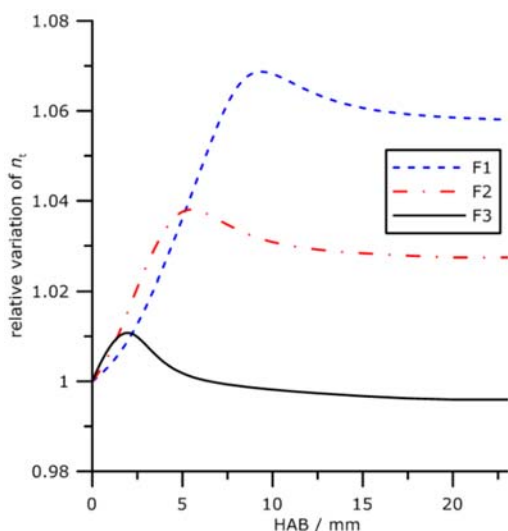


Fig. S1. Normalized variation of the total mole number along HAB in flames F1-F3. See the manuscript for the details about the flame conditions.

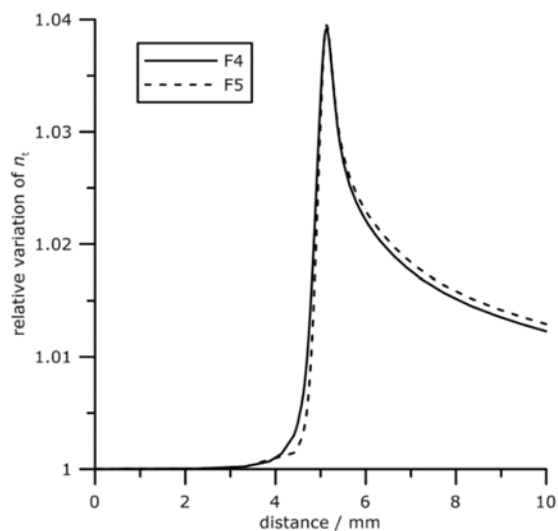


Fig. S2. Normalized variation of the total mole number along distance in flames F4 and F5. See the manuscript for the details about the flame conditions. The abscissa scale is arbitrary using “the flame speed module”. The zone of the steep gradient of n_t is coincident with the temperature gradient shown in Fig. 4 of the main manuscript.

2/ Kr-LIF thermometry in stoichiometric $\text{CH}_4/\text{O}_2/\text{N}_2$ low pressure flames F2 and F3

Figures S3 and S4 present the temperature profiles measured in flames F2 and F3, respectively stabilized at 5.3 and 10.6 kPa. Three methods have been applied; thermocouple for $T < 800$ K, NO-LIF thermometry (for details, see Lamoureux et al. [2,3]); Kr-TPLIF thermometry (present work, see the main manuscript).

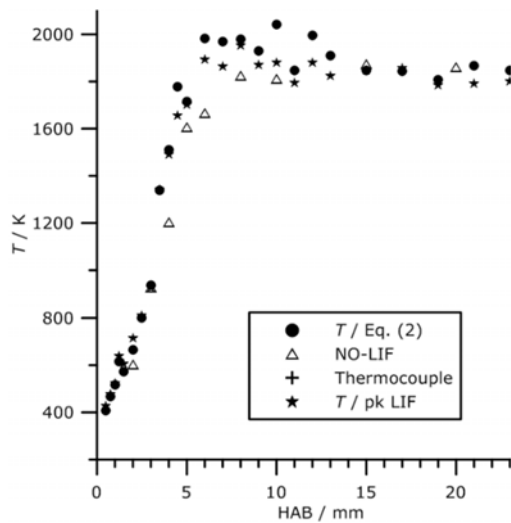


Fig. S3. Temperature profiles measured in a stoichiometric $\text{CH}_4/\text{O}_2/\text{N}_2$ flame (F2) at 5.3 kPa. Comparison with previous measurements performed with thermocouple and NO-LIF thermometry [2].

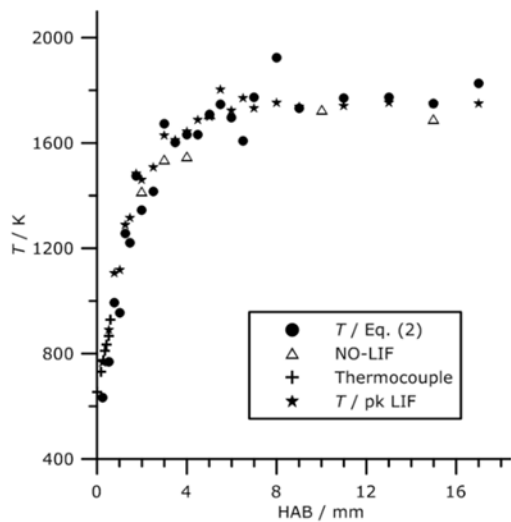


Fig. S4. Temperature profiles measured in a stoichiometric $\text{CH}_4/\text{O}_2/\text{N}_2$ flame (F3) at 10.6 kPa. Comparison with previous measurements performed with thermocouple and NO-LIF thermometry [3].

3/ Calculated quenching rate at atmospheric pressure

The quenching rate Q_{Kr} was calculated according to the temperature and the main species profiles obtained from Chemkin-Pro (for a freely propagating flame) and the collisional cross sections given by Hsu et al. [5]. Figures S5 and S6 show the comparison between the calculated Q_{Kr} and $T^{0.5}$ along the radial axis in flames F4 and F5, respectively.

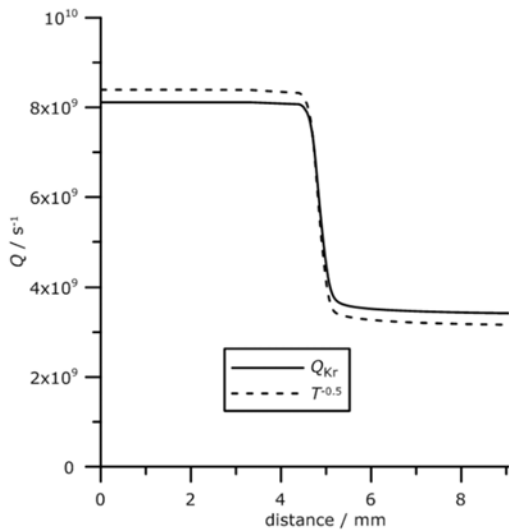


Fig. S5. Calculated quenching rate and $T^{0.5}$ as function of the radial axis in flame F4.

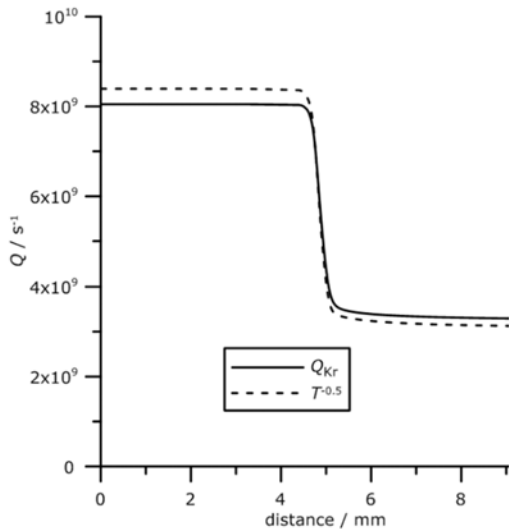


Fig. S6. Calculated quenching rate and $T^{0.5}$ as function of the radial axis in flame F5.

references

- [1] N. Lamoureux, P. Desgroux, A. El Bakali, J.F. Pauwels, Experimental and numerical study of

the role of NCN in prompt-NO formation in low-pressure $\text{CH}_4/\text{O}_2/\text{N}_2$ and $\text{C}_2\text{H}_2/\text{O}_2/\text{N}_2$ flames, *Combust. Flame.* 157 (2010) 1929–1941. <https://doi.org/10.1016/j.combustflame.2010.03.013>.

- [2] N. Lamoureux, H. El Merhubi, L. Pillier, S. de Persis, P. Desgroux, Modeling of NO formation in low pressure premixed flames, *Combust. Flame.* 163 (2016) 557–575. <http://dx.doi.org/10.1016/j.combustflame.2015.11.007>.
- [3] N. Lamoureux, P. Desgroux, In Situ Laser-Induced Fluorescence and Ex Situ Cavity Ring-Down Spectroscopy Applied to NO Measurement in Flames: Microprobe Perturbation and Absolute Quantification, *Energy Fuels.* 35 (2021) 7107–7120. <https://doi.org/10.1021/acs.energyfuels.0c03806>.
- [4] Chemkin-Pro, ANSYS, Inc., Canonsburg, PA, 2021.
- [5] A.G. Hsu, V. Narayanaswamy, N.T. Clemens, J.H. Frank, Mixture fraction imaging in turbulent non-premixed flames with two-photon LIF of krypton, *Proc. Combust. Inst.* 33 (2011) 759–766.